First-principles study on the orbital ordering of KCrF_{3}

Guangtao Wang, Zhen Li, Lihua Zheng, and Zongxian Yang

Phys. Rev. B **84**, 045111 — Published 7 July 2011

DOI: 10.1103/PhysRevB.84.045111

First principles study on the orbital ordering of $KCrF_3$

Guangtao Wang[1,2], Zhen Li[1], Lihua Zheng[1], and Zongxian Yang[1,2]
[1] *College of Physics and Information Engineering, Henan Normal University, Xinxiang, Henan 453007, Peoples Republic of China*
[2] *Henan Key Laboratory of Photovoltaic Materials, Xinxiang 453007, Peoples Republic of China*
(Dated: June 13, 2011)

The electronic, magnetic and orbital structures of $KCrF_3$ in its recently identified crystallographic phases (tetragonal and cubic) [S. Margadonna and G. Karotsis, J. Am. Chem. Soc. **128**, 16436 (2006)] are studied by first principles method. In the tetragonal phase, both the generalized gradient approximation (GGA) and the GGA+U calculations show that the ground state is the A-type antiferromagnetic (A-AFM) configuration with G-type orbital ordering pattern. Our calculations show that the orbital structures and the magnetic configurations can be measured by the optical conductivity. In the cubic state, the GGA calculations show that the ground state is a ferromagnetic half metal state, while the GGA+U (U_{eff}=3.0 eV) calculations show that the A-AFM insulator phase is the ground state. Our calculations indicate that the electron-electron interactions rather than the electron-phonon interactions are the driving forces behind the orbital ordering.

PACS numbers: 74.25.Ha, 71.18.+y, 71.20.-b

I. INTRODUCTION

The strongly correlated electron systems such as the 3d transition-metal oxides have attracted considerable attention, where orbital, charge, and spin degrees of freedom play important roles in the electronic, magnetic, and transport properties. In particular, the orbital degree of freedom and the orbital orderings give rise to very rich physics properties[1–6]. The well-known examples for such ordering phenomena are the perovskite-based manganites $La_{1-x}A_xMnO_3$ (A=Ba, Sr, and Ca)[7,8]. The undoped parent compound $LaMnO_3$ is known[5] to be an A-type antiferromagnetic (AFM) insulator in which the orbital ordering is formed due to the cooperative Jahn-Teller effect. The electronic configuration of the Mn^{3+} ions in $LaMnO_3$ is $t_{2g}^3e_g^1$, where the three electrons in the t_{2g} orbitals are localized with a total spin of $3\mu_B$, while the itinerary electron in one of e_g atomic orbitals is strongly hybridized with the neighboring O-2p orbitals. This particular orbital ordering is responsible for the A-type antiferromagnetic structure of $LaMnO_3$. Besides the transition-metal oxides, the transition-metal fluorides also exhibit the intriguing electronic and magnetic effects. However, compared with the extensive studies of the oxides, the study of the fluorides is still lacking due to the difficulty of synthesis. $KCrF_3$ is one kind of the perovskite structure fluorides in which the electronic and structural characteristics are expected to resemble those of $LaMnO_3$ since the orbital degrees of freedom are activated for Cr^{2+} (d^4), which is isoelectronic analogue of Mn^{3+} (d^4) in $LaMnO_3$. Recently, Margadonna and Karotsis[9] investigated the structural and magnetic properties of $KCrF_3$. Both the structural and magnetic phase transitions seem to be more complex than expected. The $KCrF_3$ displays not only the large cooperative Jahn-Teller distortions at room temperature but also a series of temperature induced structural and magnetic transformations.

Although several experimental and theoretical results have been reported about $KCrF_3$[9–13], no one has clearly seen the orbital ordering. This may be because the direct observation of orbital structure is difficult. However, several experiments[14–19] have been developed to detect the anisotropy induced by the spin and orbital orderings. Among them, the measurement of anisotropic optical conductivity[16–18] using polarized light could provide us with some useful information. Here, we reported the optical conductivity calculated from first-principles[20]. Our calculated optical conductivity indicated that its orbital and magnetic order could be measured in this way.

Typically, the origin of the orbital polarization is believed to be the electron-phonon interaction (the Jahn-Teller distortion)[21] and the electron-electron interaction[22,23]. To establish the origin of the orbital ordering in $KCrF_3$, we performed calculations without Jahn-Teller distortion but including electron-electron correlations. The existence of orbital order indicates that the electron-electron interactions rather than the electron-phonon interactions are the driving forces behind the orbital ordering.

II. METHOD AND DETAILS

The calculations were done with the BSTATE[24] code, in the ultra-soft pseudopotential plane wave method. All the lattice constant and the atomic positions adopted in our calculations are borrowed from the experiment[9]. After carefully checking the convergence of the calculated results with respect to the cutoff energy and the number of k-points, we adopted a cutoff energy of 30 Ry and Monkhorst-Pack k-points generated with a $16 \times 16 \times 12$ grid. In order to determine the true ground state, we have considered four different cases, including the ferromagnetic (FM), and the three different antiferromagnetic (AFM) spin configurations. The first AFM configuration is the A-type antiferromagnetic (A-AFM), where the spins of Cr^{2+} are parallel in the a-b plane and antiparallel along the c-axis. The second one is the C-type antiferromagnetic (C-AFM), where the spins of Cr^{2+} are parallel along the c-axis and antiparallel in the a-b plane. The third one is the G-type antiferromagnetic (G-AFM), where the spins of Cr^{2+} are antiparallel to all the nearest neighbors. The various magnetic structures are schematically shown in Fig.1. As for the exchange-correlation potential, we adopted the generalized gradient approximation (GGA) by using the Perdew-Burke-Ernzerhof scheme[25].

The first-principle calculations based on the density-functional theory have been well developed and widely accepted as a powerful theoretical tool for explaining and predicting the ground state properties and the electronic structures of a large amount of materials such as simple metals and band insulators. Nevertheless, the theoretical understanding has been hindered by the well-known deficiencies[26]: 1. the nonlocality of the screened exchange interaction is not taken into account and the electrostatic self-interaction is not entirely compensated; 2. the Kohn-Sham gap is usually a factor of 2-3 smaller than the fundamental gap of the solid. To overcome the second deficiency, Anisimov developed the GGA+U corrections[27], where the on-site interaction was treated in a static Hartree mean-field manner. It is suited for strongly correlated systems with long-range ordering, such as the antiferromagnetic ordered insulators. Recently, a new and powerful method called *Hybrid functionals*[28] has been developed. This method overcomes the two deficiencies discussed above to a large extend[29] and can be used in metals, semiconductors and transition metal monoxides. Such Hybrid functional ideas can also be used in the DFT+U method, where the U parameter was replaced with the adjustable Fock exchange[30].

As mentioned above, the anisotropic optical conductivity[16–18,20] could provide us with some useful information about orbital ordering. The inter-band optical conductivity is calculated from the converged Kohn-Sham wave functions $|\psi_{n\mathbf{k}}\rangle$ and eigen values $E_n(\mathbf{k})$ by using the following Kubo formula[20,31] (in Ry units):

$$\begin{aligned}\sigma_{\alpha\beta}(\omega) &= -\frac{16}{V}\sum_{\mathbf{k}n} i f_{n\mathbf{k}} \sum_m \frac{1}{\omega_{mn}^2 - (\omega + i\delta)^2} \\ &\left[\frac{\omega + i\delta}{\omega_{mn}} Re(\pi_{nm}^{\alpha}\pi_{mn}^{\beta}) + iIm(\pi_{nm}^{\alpha}\pi_{mn}^{\beta})\right] \end{aligned} \quad (1)$$

where α and β $(=x, y, z)$ are indices for directions, ω is the excitation energy, V is the volume of the unit cell, n and m are band indices, $f_{n\mathbf{k}}$ is the Fermi distribution function, $\omega_{mn} = E_m(\mathrm{k}) - E_n(\mathrm{k})$ and δ is the lifetime broadening (δ=0.01Ry in this work), $\pi_{nm}^{\alpha} = \langle\psi_{n\mathbf{k}}|(-i\nabla_{\alpha})|\psi_{m\mathrm{k}}\rangle$ are the matrix elements of the momentum operator.

III. RESULTS AND DISCUSSION

A. Electronic structure of the tetragonal phase

The total energies and magnetic moments of the different magnetic states are calculated by using both the GGA and GGA+U schemes. The calculated results are presented in Table I. It can be seen that the A-AFM phase is the ground state, which is in good agreement with the neutron diffraction results[13] and the calculated results by Xu[12] and Giovannetti[11]. With U_{eff}=0.0 eV, there exists a small difference in the total energies between the A-AFM and FM states (0.024 eV/ f.u.), while the energy differences between the A-AFM and the other two AFM configurations, namely, C-AFM and G-AFM, are about 0.260 and 0.259 meV/ f.u., respectively.

It is recalled that the A-AFM and the FM structures have a ferromagnetic a-b plane but a different stacking along the c axis, whereas both the C-AFM and G-AFM states are antiferromagnetically ordered in the a-b plane but have an opposite stacking in the c-axis direction. This reveals that the ferromagnetic exchange interactions in the a-b plane are more favorable and robust than those along the c-axis direction, indicating a strong two-dimensional character for $KCrF_3$. In order to calculate the exchange interactions in the a-b plane (J_{ab}) and along the c-axis (J_c), we approximately decouple the spin degree of freedom and treat it in term of the Heisenberg model, then the exchange

interaction can be estimated by mapping the calculated total energies for each magnetic state[32], E(F), E(A), E(C) and E(G), to the Heisenberg model. So, the nearest neighboring exchange coupling constants are given by:

$J_c = [E(F) - E(G) - E(A) + E(C)]/(4S^2)$

$J_{ab} = [E(F) - E(G) + E(A) - E(C)]/(8S^2)$

where S=3.5 is the moment of Cr^{2+}. From calculated results, we can see that J_{ab} are much larger than J_c, especially with smaller U_{eff}. The difference in total energy between the A-AFM and FM, C-AFM, G-AFM states decreases with increasing correlation (U_{eff}), accompanying decreasing exchange interactions J_{ab}. While the exchange interactions along the c-axis (J_c) and the moments of the Cr ions are hardly changed with the correlation (U_{eff}). The positive J_{ab} and negative J_c indicate the ferromagnetic coupling in the a-b plane and antiferromagnetic along the c-axis, respectively.

As mentioned above, the true ground state of $KCrF_3$ is the A-AFM state, so we presented its density of states (DOS) in Fig.2. The states from -10.0 to -6.0 eV are mostly derived from F-2p, while the DOS around the Fermi level are mostly derived from up-spin Cr-3d states, leaving the down-spin states empty in the range from 1.5 to 4.0 eV. For the divalent Cr^{2+} ion, it is in the center of octahedron around by six F atoms. So the Cr-3d states split into three low energy t_{2g} and two high energy e_g states. Our results indicated that the four electrons of the Cr^{2+} ion occupied the three t_{2g} states and one orbital of the e_g states ($t_{2g}^3 e_g^1$). That is to say, it is in the high-spin configuration, which is consistent with the Hund's rule and with the experimental measurements[9,13]. From the X-ray and neutron diffractions[10], we know that the system is the cubic perovskite at very high temperature (973K), below which the high spin Cr^{2+} ion induces a lattice distortion to a body-centered tetragonal unit cell (space group I4/mcm). In the tetragonal phase, the CrF_6 octahedra are distorted, leading to short Cr-F bonds along the c axis and alternating long-short Cr-F bonds in the a-b plane, indicative of the presence of a staggered type of orbital ordering. Such orbital ordering can be clearly seen in Fig.3.

In Fig.3(a), for Cr_1 (see Fig.1), three electrons occupy the up-spin t_{2g} states and one electron occupies the up-spin $d_{3x^2-r^2}$ state. The $d_{z^2-y^2}$ state lying 0.5 eV above the Fermi level, is empty. For Cr_2, all the up-spin t_{2g} states and one of the e_g ($d_{3y^2-r^2}$) states are occupied, leaving the up-spin $d_{z^2-x^2}$ orbital empty. For Cr_3, all the down-spin t_{2g} states and the $d_{3y^2-r^2}$ orbital are occupied. Such orbital ordering is consistent with the Goodenough-Kanamori-Anderson rules, where the e_g- e_g exchange interaction within the a-b plane is FM due to a virtual electron hopping between an occupied and an empty orbital via the intermediate F ligand, while the half-filled orbitals of t_{2g}-t_{2g} exchange through the medial F atoms between the planes is AFM.

As we mentioned before, the direct observation of the orbital structure is difficult. However, the measurement of the anisotropic optical conductivity has been proved to be a useful way to measure the orbital structure indirectly. The calculated optical conductivity (see Fig.3(d)) has a signature that may be referred to the underlying orbital ordering. In the a-b plane, the optical conductivity $\sigma_{\parallel}$ has two peaks, with α_1 at 1.0 eV and α_2 at about 8.0 eV, respectively. The peak α_1 is derived from electrons hopping between the occupied $d^{\uparrow}_{3x^2-r^2}$ of Cr_1 and the unoccupied $d^{\uparrow}_{z^2-x^2}$ of Cr_2. Along the c-axis, this peak does not exist. If the electron on the occupied $d^{\uparrow}_{3x^2-r^2}$ of Cr_1 hop to the $d^{\downarrow}_{z^2-x^2}$ of Cr_3, it has to change its spin direction, which would seldom happen. The peak α_2 comes from the electrons hopping between the F_1-2p orbitals and the unoccupied $d_{z^2-x^2}$ (or $d_{z^2-y^2}$). Along the c-axis, the electron in the 2p state of F_2 (at the apex of the CrF_6 octahedron) can also hop to unoccupied $d_{z^2-x^2}$ (or $d_{z^2-y^2}$), so such optical conductivity peak also appears in $\sigma_{\perp}$ at 9.0 eV (β_3). Along the c-axis, besides peak β_3, there are two peaks with β_1 at 3.3 eV and β_2 at 6.8 eV. From the projected DOS (PDOS), we know that the peak β_1 is derived from electrons hoping between the $d^{\uparrow}_{3x^2-r^2}$ of Cr_1 and the $t^{\uparrow}_{2g}$ of Cr_3. The peak β_2 comes from electrons hoping between the $d^{\uparrow}_{3x^2-r^2}$ of Cr_1 and the $d^{\uparrow}_{z^2-x^2}$ of Cr_3.

In order to properly describe the strong electron correlation for the Cr-3d electron of $KCrF_3$, we calculated its electronic structure with the GGA+U method. We use an effective U parameter of U_{eff}=3.0 eV (U=4.0 and J=1.0 eV), which has been proved to be a suitable parameter by previous works[12,33–35]. We also performed further calculations with different U_{eff} values (0.0, 1.0, 2.0, 4.0, and 5.0 eV) and found that both the energy difference and the exchange constant in the a-b plane (J_{ab}) decrease with the increasing of U_{eff} (see Table I). The total density of state and PDOS of $KCrF_3$ calculated with U_{eff}=3.0 eV are presented in Fig.4, where the states of the occupied Cr-3d are pushed down (from -4.0 to -2.0 eV), comparing with the GGA results, while the states of the F-2p are hardly changed.

The calculated PDOS and optical conductivity with U_{eff}=3.0 eV are presented in Fig.5, which are similar to those in Fig.3, excepting the gap between the occupied $d_{3x^2-r^2}$ and the unoccupied $d_{z^2-x^2}$ states increased from 0.6 eV to 2.2 eV. At the same time, all the optical conductivity peaks shifted to higher energy. In Fig.5(d), the peak α_1 and peak α_2 lie at about 2.7 eV and 9.0 eV, respectively. The peak β_1, β_2, and β_3 are located near 5.5 eV, 7.5 eV, and 9.0 eV, respectively. The correlation is a very complicated concept and beyond the simple Hubbard model correction of the DFT+U method. However, the optical conductivity can provide the information of the d-d transition band gap[36], which was regard as the electron correlation approximately[37].

To clearly show the existence of the orbital ordering in the tetragonal A-AFM phase, we presented the spin resolved charge density in Fig.6. Where the x, y and z axis are along the [1 $\bar{1}$ 0], [110], and [001] directions of the unit cell, respectively. For the occupied states (Left part of Fig.6), the $d_{3x^2-r^2}$ and the $d_{3y^2-r^2}$ orbital staggered in the a-b plane, while along the c-axis the $d_{3x^2-r^2}$ of Cr_1 is rotated by 90 degree to $d_{3y^2-r^2}$ on Cr_3. So the G-type orbital ordering is formed. For the unoccupied states (in the range from 0.0 eV to 2.0 eV), the G-type orbital ordering is formed by the $d_{z^2-x^2}$ and $d_{z^2-y^2}$ orbital (Right part of Fig.6).

Generally the magnetic ordering is measured by neutrons, just as Xiao[13] who using this method determined the A-AFM phase as the ground state for $KCrF_3$. However, we find optical that conductivity measurement can also determine the magnetic ordering. In Fig.7, we show the calculated optical conductivity of different magnetic phases. In the A-AFM (Fig.7(a)) and the FM (Fig.7(c)) phases, where the ferromagnetic ordering preserves in the a-b plane, which provides the passageway for the electron hopping from the Cr_1 ($d^{\uparrow}_{3x^2-r^2}$) to the Cr_2($d^{\uparrow}_{z^2-x^2}$). So the peak α_1 appears in both phases. Along the c-axis, the electron on the Cr_1-$d^{\uparrow}_{3x^2-r^2}$ orbital can not hop to the Cr_3-$d^{\downarrow}_{z^2-x^2}$, since the spin directions of two orbitals are antiparallel in the A-AFM phase. However, the two orbitals are parallel in FM phase, so there is a peak β_1 at the same position as peak α_1 in Fig.7(c). For the case of the C-AFM, it is ferromagnetic along the c-axis and antiferromagnetic in the a-b plane. So the electron hopping from the Cr_1-$d^{\uparrow}_{3x^2-r^2}$ to the Cr_3-$d^{\uparrow}_{z^2-x^2}$ brings about the peak β_1 at about 2.8 eV. For C-AFM, it is antiferromagnetism in the a-b plane, the electron on Cr_1-$d^{\uparrow}_{3x^2-r^2}$ can not hop to Cr_2-$d^{\downarrow}_{z^2-x^2}$, because of the antiparallel spin direction. The electron on Cr_1-$d^{\uparrow}_{3x^2-r^2}$ can hop to Cr_2-$t^{\uparrow}_{2g}$, which results in the peak α_1 at about 5.5 eV. In the G-AFM phase, it is antiferromagnetic in both the a-b plane and along the c-axis, which prevented the electron hopping from Cr_1-$d^{\uparrow}_{3x^2-r^2}$ to Cr_2-$d^{\downarrow}_{z^2-x^2}$(Cr_2-$d^{\downarrow}_{z^2-y^2}$). So, no peak appears in both the a-b plane and along the c-axis at 2.8 eV. The optical conductivity peaks appear at about 5.5 eV (α_1, and β_1) come from electron hopping from Cr_1-$d^{\uparrow}_{3x^2-r^2}$ to Cr_2-$t^{\uparrow}_{2g}$ and to Cr_3-$t^{\uparrow}_{2g}$. From the above discussion, it shows that we can determine the magnetic ordering and the electron correlation by measuring the position of optical conductivity peaks.

B. Cubic phase: The Origin of the orbital polarization

The mechanism responsible for the orbital ordering is still being debated in the literature[21,22]. Some researchers ascribe the origin of the orbital polarization to the electron-phonon interaction (Jahn-Teller distortion)[21], while other researchers attribute the origin to the electron-electron interaction[22]. So, it is important to study the mechanism responsible for the orbital order in $KCrF_3$. When the temperature is higher than 973K, the $KCrF_3$ enters into the cubic phase, where all the Cr-F bonds distance are equal. If the Jahn-Teller distortion is the origin of the orbital polarization, the orbital ordering would disappear, which was suggested by Margadonna[10]. However, some theoretical calculations[38] on $KCuF_3$ indicate that the orbital polarization excites even without Jahn-Teller distortion. This means that the origin of the orbital polarization should be the electron-electron interaction. Therefore, there is a great need to study the orbital polarization and magnetism of $KCrF_3$ in the cubic state.

In Table.II, the total energies (with respect to the A-AFM state) of the FM, C, and G-type antiferromagnetic states are presented. For the electron correlation of $U_{eff} \leq 2.0$ eV, the FM state is the most stable state, while the A-AFM state becomes the ground state for $U_{eff} \geq 3.0$ eV . The calculated exchange constants, J_{ab} and J_c, are positive with $U_{eff} \leq 2.0$ eV, which indicates the ferromagnetic coupling in both the a-b plane and along the c-axis. For $U_{eff} \geq 3.0$ eV, J_c becomes negative, which means the magnetic coupling along the c-axis is antiferromagnetic. The values of J_{ab} are three times as that of J_c, which means that the ferromagnetic couplings in the a-b plane are much stronger than those along the c-axis.

Since the ground state is the A-AFM state with $U_{eff} \geq 3.0$ eV, we present the projected density of states of Cr in Fig.8. In the GGA formula (Fig.8(a)), the three t_{2g} orbitals are fully occupied, while the two e_g orbitals are half filled. In the cubic phase, the JT distortion disappears, therefore the two e_g orbitals, $d_{3z^2-r^2}$ and $d_{x^2-y^2}$, are almost degenerate, without considering the electron correlation. Such electronic structure is consistent with Margadonna's[10] suggestion. However, when the electron correlation is included with U_{eff}=3.0 eV, $KCrF_3$ enters into the orbital ordering Mott-insulator phase, as shown in Fig.8(b). The four electrons of Cr^{2+} filled the three t_{2g} orbitals and the $d_{x^2-y^2}$ orbital. Such result means that, even without the JT distortion, the orbital polarization arises in $KCrF_3$ as long as the electron correlation is included. So our calculations indicate that the origin of the orbital polarization is

the electron-electron interaction, which is in agreement with Anisimov's results on $KCuF_3$[38]. From Table.II we can see that the occupation number of the $d_{x^2-y^2}$ orbital increases from 0.5 (U=0.0 eV) to 1.0 (U=4.0 eV), at the same time, the occupation number of $d_{3z^2-r^2}$ orbital decreases from 0.5 to 0.0.

As mentioned above the electron-phonon interaction (Jahn-Teller distortion) can also cause orbital polarization[21]. So we show the occupation numbers of $d_{x^2-y^2}$ and $d_{x^2-y^2}$ with different values of the Jahn-Teller distortion in Fig.9. The Jahn-Teller distortion ratio is defined as[23] $\delta_{JT}=\frac{d_1-d_s}{d_1+d_s}$, where d_1 and d_s denote the long and short Cr-F bond distances. From Fig.9, we can see that the occupation number of $d_{x^2-y^2}$ increases with δ_{JT} increasing, which indicates that the Jahn-Teller distortion favors orbital polarization. However, the Jahn-Teller distortion is not the determinant factor on orbital polarization. For $U_{eff} < 2.0$ eV, completely orbital polarization does not take place even with Jahn-Teller distortion δ_{JT} as large as 0.14. The insert figure in Fig.9 shows polarization increases with the JT distortion δ_{JT} at different electron correlations (U_{eff}). The polarization is defined as $N_{x^2-y^2}$-$N_{3z^2-r^2}$, where $N_{x^2-y^2}$ and $N_{3z^2-r^2}$ are the occupation numbers of $d_{x^2-y^2}$ and $d_{3z^2-r^2}$ orbitals, respectively. From the insert figure of Fig.9, we can see that complete polarization takes place even without the Jahn-Teller distortion when $U_{eff} \geq 3.0$ eV. Therefore, we may draw the conclusion that the electron correlation is the origin of the orbital polarization, while the Jahn-Teller distortion reinforces such polarization.

C. Summary and Conclusion

In summary, by performing first principles calculation, we studied the electronic, magnetic and orbital structures of the $KCrF_3$ in the tetragonal and cubic phases. In the tetragonal phase, both the GGA and GGA+U calculations show that the ground state is the A-type AFM configuration with the G-type orbital ordering. Such orbital ordering can be well understood by the calculated optical conductivity. The calculated exchange constant J_{ab} is about three times of J_c, which indicates the strong two-dimensional character. In the cubic state, the GGA calculations show that the ground state is a FM half metallic state, while the GGA+U (U_{eff}=3.0 eV) calculations show that the A-AFM state is the ground state. By studying how the orbital polarization changes with the electron correlation and the Jahn-Teller distortion, we found that the origin of the orbital polarization should be the electron correlation and the Jahn-Teller distortion can reinforced such polarization. Such results is in accordance with Anisimov's results on the $KCuF_3$[38].

Acknowledgments

The authors acknowledge the supports from NSF of China (No.10947001) and the Innovation Scientists and Technicians Troop Constriction Projects of Henan Province (Grant No. 104200510014). The authors appreciate Professor P. J. Ford and F. G. Chang for fruitful discussions and improving the English.

[1] M. Imada, A. Fujimori, and Y. Tokura, Rev. Mod. Phys. **70**,1039 (1998); E. Dagotto, ibid. **66**, 763 (1994).
[2] P. A. Lee, N. Nagaosa, and X. Wen, Rev. Mod. Phys. **78**,17 (2006).
[3] Y. Tokura and N. Nagaosa, SCIENCE **288**, 462 (2000); T. Kimura, T. Goto, H. Shintani, K. Ishizaka, T. Arima, and Y. Tokura, NATURE **426**, 55 (2003).
[4] S. T. Lou, F. M. Zimmermann, R. A. Bartynski, N. Hur, and S. W. Cheong, Phys. Rev. B **79** 214301 (2009).
[5] H. Y. Hwang, S. W. Cheong, P. G. Radaelli, M. Marezio, and B. Batlogg, Phys. Rev. Lett. **75**, 914 (1995); S. Yunoki, T. Hotta, and E. Dagotto, ibid. **84**, 3714 (2000); I. A. Sergienko, C. Sen, and E. Dagotto, ibid. **97**, 227204 (2006).
[6] S. Kümmel and L. Kronik, *Rev. Mod. Phys.* **80**, 3 (2008).
[7] A. Asamitsu, Y. Moritomo, Y. Tomioka, T. Arima, and Y. Tokura, Nature **373**, 407 (1995).
[8] I. S. Elfimov, V. I. Anisimov, and G. A. Sawatzky, Phys. Rev. Lett. **82**, 4264 (1999).
[9] S. Margadonna and G. Karotsis, J. Am. Chem. Soc. **128**, 16436 (2006).
[10] S. Margadonna and G. Karatsis, J. Mater. Chem, **17**, 2013 (2007).
[11] G. Giovannetti, S. Margadonna, and J. Brink, Phys. Rev. B **77**, 075113 (2008).
[12] Y. Xu, X. Hao, M. Lv, Z. Wu, D. Zhou, and J. Meng, J. Chem. Phys. **128**, 164721 (2008).
[13] Y. Xiao, Y. Su, H. F. Li, C. M. N. Kumar, R. Mittal, J. Persson, A. Senyshyn, K. Gross, and Th. Brueckel, Phys. Rev. B **82**, 094437 (2010).
[14] Y. Murakami, J. P. Hill, D. Gibbs, and *et al.*, Phys. Rev. Lett **81**, 582 (1998).
[15] E. Saitoh, S. Okamoto, K. T. Takahashi, and *et al.* Nature **410**, 180 (2001).
[16] Y. Okimoto, Y. Tomioka, Y. Onose, and *et al.*, Phys. Rev. B **59**, 7401 (1999).
[17] K. Tobe, T. Kimura, Y. Okimoto, and K. Tokura, Phys. Rev. B **64**, 184421 (2001).
[18] J. Deisenhofer, I. Leonov, M.V. Eremin, Ch. Kant, P. Ghigna, F. Mayr, V.V. Iglamov, V. I. Anisimov, and D. van der Marel, Phys. Rev. Lett. **101**, 157406 (2008); S. Ishihara, M. Yamanaka, and N. Nagaosa, Phys. Rev. B **56**, 686 (1997); W. Z. Hu, J. Dong, G. Li, Z. Li, P. Zheng, G. F. Chen, J. L. Luo, and N. L. Wang, Phys. Rev. Lett. **101**, 257005 (2008).
[19] E. Benckiser, M. W. Haverkort, S. Brück, et al., Nat. Mat. **10**, 189 (2011).
[20] A. Stroppa, S. Picozzi, A. Continenza, M. Y. Kim, A. J. Freeman, Phys. Rev. B **77**, 235208 (2008).
[21] D. I. Khomskii and K. I. Kugel, Solid State Commun. 13, 763 (1973); I. Loa, P. Adler, A. Grzechnik, K. Syassen, U. Schwarz, M. Hanfland, G. Kh. Rozenberg, P. Gorodetsky, and M. P. Pasternak Phys. Rev. Lett. **87**, 125501 (2001); Z. Popović and S. Satpathy, Phys. Rev. Lett. **88**, 197201 (2002).
[22] I. Leonov, N. Binggeli, Dm. Korotin, V. I. Anisimov, N. Stojić, and D. Vollhardt, Phys. Rev. Lett. **101**, 096405 (2008); J. E. Medvedeva, M. A. Korotin, V. I. Anisimov, and A. J. Freeman, Phys. Rev. B **65**,172413 (2002).
[23] J. E. Medvedeva, M. A. Korotin, V. I. Anisimov, and A. J. Freeman, Phys. Rev. B **65**, 172413 (2002); I. Leonov, Dm. Korotin, N. Binggeli, V. I. Anisimov, and D. Vollhardt, Phys. Rev. B **81**,075109 (2010).
[24] Z. Fang and K. Terakura, *J. Phys.: Condens. Matter* **14**, 3001 (2002).
[25] John P. Perdew and Yue Wang, *Phys. Rev. B* **45**, 13244 (1992).
[26] A. Stroppa and G. Kresse, *Phys. Rev. B* **79**, 201201 (2009).
[27] V. I. Anisimov, J. Zaanen, and O. K. Anderson, *Phys. Rev. B* **44**, 943 (1991); V. I. Anisimov, I. V. Solovyev, M. A. Korotin, M. T. Czyzyk and G. A. Sawatzky, *Phys. Rev. B* **48**, 16929 (1993); I. V. Solovyev, P. H. Dederichs, and V. I. Anisimov, *Phys. Rev. B* **50**, 16861 (1994). A. I. Liechtenstein, V. I. Anisimov, and J. Zaanen, *Phys. Rev. B* **52**, R5467 (1995); V. I. Anisimov, F. Aryasetiawan, and A. I. Liechtenstein, *J. Phys.: Condens. Matter* **9**, 767 (1997); H. Sawada, Y. MorikawaK. Terakura and N. Hamada *Phys. Rev. B* **56**, 12154 (1997).
[28] J. Paier, R. Hirschl, M. Marsman, and G. Kresse, *J. Chem. Phys.* **122**, 234102 (2005); J. Heyd, J. E. Peralta, G. E. Scuseria, and R. L. Martin, ibid. **123**, 174101 (2005); J. Paier, M. Marsman, K. Hummer, G. Kresse, I. C. Gerber, and J. G. ángyán, ibid. **124**, 154709 (2006); J. Paier, M. Marsman, and G. Kresse, ibid. **127**, 024103 (2007); M. Marsman, J. Paier, A. Stroppa, and G. Kresse, J. Phys.: Condens. Matter **20**, 064201 (2008); A. Stroppa and G. Kresse, New J. Phys. **10**, 063020 (2008).
[29] J. Heyd and G. E. Scuseria, *J. Chem. Phys.* **118**, 8207 (2003); B. G. Janesko, T. M. Henderson, and G. E. Scuseria, ibid. **130**, 081105 (2009); B. G. Janesko, T. M. Henderson, and G. E. Scuseria, ibid. **131**, 034110 (2009); Joachim Paier, C. V. Diaconu, G. E. Scuseria, M. Guidon, J. V. Vondele,and J. Hutter, *Phys. Rev. B* **80**, 174114 (2009). B. G. Janesko, T. M. Henderson and G. E. Scuseria, Phys. Chem. Chem. Phys. **11**, 443 (2009); A. Stroppa and S. Picozzi, ibid. **12**, 5405 (2010); J. L. F. Da Silva, M. V. Ganduglia-Pirovano, J. Sauer, V. Bayer, and G. Kresse, *Phys. Rev. B* **75**, 045121 (2007); L.-L. Wang and D. D. Johnson, ibid. **75**, 235405 (2007);
[30] B. Meredig, A. Thompson, H. A. Hansen, and C. Wolverton, *Phys. Rev. B* **82**, 195128 (2010).
[31] C. S. Wang and J. Callaway, *Phys. Rev. B* **9**, 4897 (1974).
[32] K. F. Wangab , J. M. Liuab and Z. F. Ren, *Adv. Phy.* **58**, 321 (2009); Z. Fang and N. Nagaosa, Phys. Rev. Lett. **93**, 176404 (2004); P. Rivero, I. P. R. Moreira and Francesc Illas, J. of Phys.: Conference Series **117** 012025 (2008); I. P. R. Moreira and Francesc Illas, *Phys. Rev. B* **55**, 4129 (1997); I. P. R. Moreira and Francesc Illas, Phys. Chem. Chem. Phys. **8** 1645 (2006).
[33] M. A. Korotin, V. I. Anisimov, D. I. Khomskii, and G. A. Sawatzky, Phys. Rev. Lett. **80**, 4305 (1998).
[34] K.-W. Lee and W. E. Pickett, Phys. Rev. B **80**, 125133 (2009).
[35] H. Weng, Y. Kawazoe, X. Wan, and J. Dong, Phys. Rev. B **74**, 205112 (2006).
[36] J. Matsuno, Y. Okimoto, M. Kawasaki, and Y. Tokura, Phys. Rev. Lett. **95**, 176404 (2005).
[37] T. Arima, Y. Tokura, and J. B. Torrance, *Phys. Rev. B* **48**, 17006 (1993); J. Zaanen, G. A. Sawatzky, J. W. Allen, Phys. Rev. Lett. **55**, 418 (1985).

[38] I. Leonov, Dm. Korotin, N. Binggeli, V. I. Anisimov, and D. Vollhardt, Phys. Rev. B **81**, 075109 (2010).

Figures

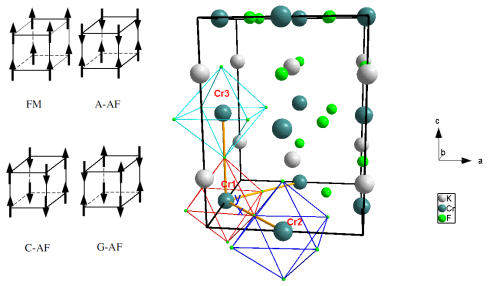

FIG. 1: (color online) (Right) The tetragonal structure (space group I4/mcm) of $KCrF_3$. We defined x, y and z axis as the [1 $\bar{1}$ 0], [110], and [001] direction of the unit cell respectively. (Left) Various magnetic structures are schematically shown.

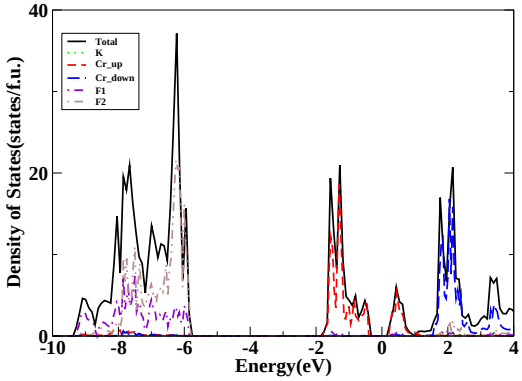

FIG. 2: (color online) The density of states of $KCrF_3$ calculated with GGA in the tetragonal A-AFM structure.

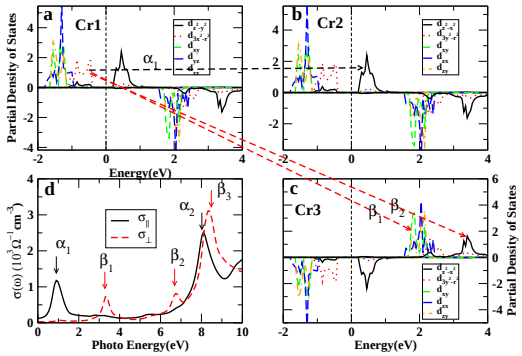

FIG. 3: (color online) The projected density of states of Cr1 (a), Cr2 (b), Cr3 (c) and the calculated optical conductivity (d) of $KCrF_3$ with GGA in the tetragonal A-AFM structure. Where the $\sigma_{\parallel}$ means optical conductivity in a-b plane, while the $\sigma_{\perp}$ means optical conductivity along c-axis.

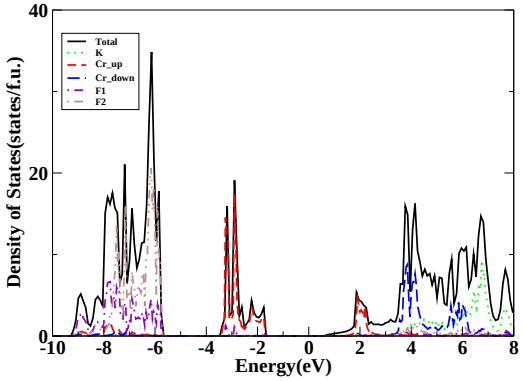

FIG. 4: (color online) The density of states of $KCrF_3$ calculated with GGA+U (U=4.0 eV, J=1.0 eV) in the tetragonal A-AFM structure.

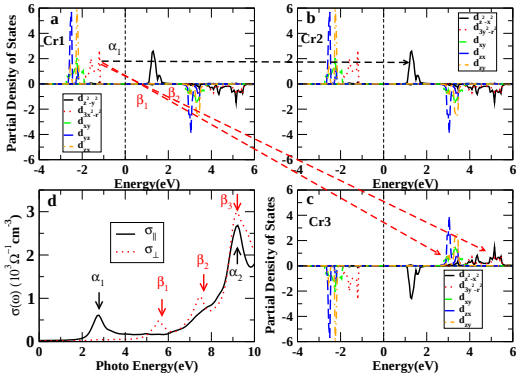

FIG. 5: (color online) (The projected density of states of Cr1 (a), Cr2 (b), Cr3 (c) and the calculated optical conductivity (d) of $KCrF_3$ with GGA+U (U=4.0 eV, J=1.0 eV) in the tetragonal A-AFM structure.

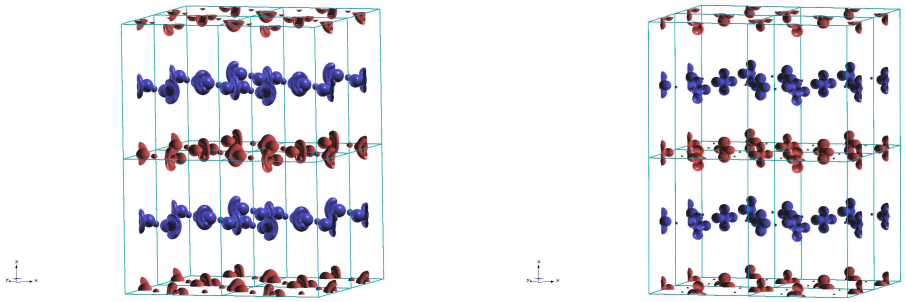

FIG. 6: (color online) Spin resolved charge density at the region extending from -2.0 eV to 0.0 eV (Left) and from 0.0 eV to 2.0 eV (Right), using results of GGA+U (U=4.0 eV, J=1.0 eV) for A-AFM in the tetragonal structure. The x, y and z axis are along the [1 $\bar{1}$ 0], [110], and [001] direction of the unit cell, respectively.

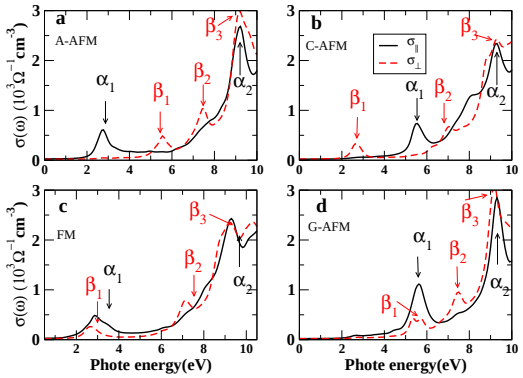

FIG. 7: (color online) (a)The calculated optical conductivity of $KCrF_3$ for A-AFM phase (a), C-AFM phase (b),FM phase (c) and G-AFM phase (d), with GGA+U (U=4.0 eV, J=1.0 eV).

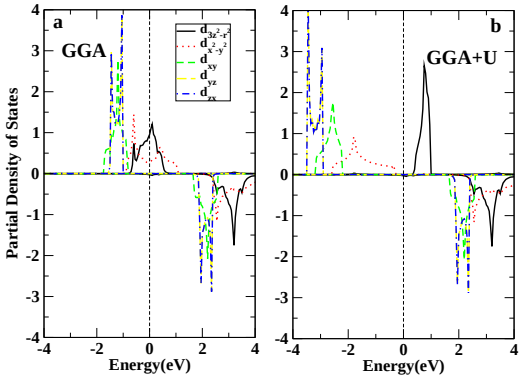

FIG. 8: (color online) The projected density of states of Cr in cubic structure for The A-AFM phase, with GGA (a) and GGA+U (U=4.0 eV, J=1.0 eV)(b).

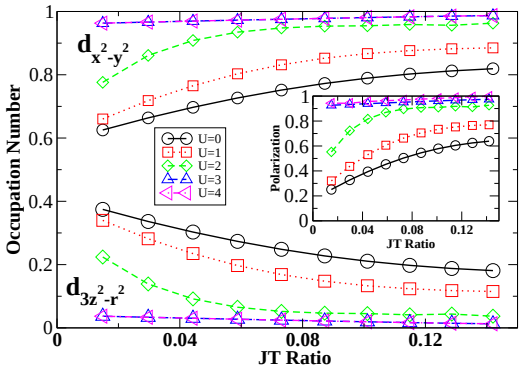

FIG. 9: (color online) The occupation numbers of $d_{3z^2-r^2}$ and $d_{x^2-y^2}$, at U=0.0, 1.0, 2.0, 3.0 and 4.0 eV, varying with JT ratio.

Tables

TABLE I: The total energy of the FM, C, G-type antiferromagnetism (with respect to A-AFM), the exchange constant in the a-b plane (J_{ab}) and along the c-axis J_c, the moment of the Cr ion and the band gap of the A-AFM state, varying with the correlation (U_{eff}).

U_{eff}	FM(meV)	C(meV)	G(meV)	J_{ab}(meV)	J_c(meV)	Moment(μ_B)	gap(eV)
0	24	261	258	5.3	-0.6	3.51	0.57
1	13	178	165	3.6	-0.6	3.54	1.11
2	15	116	108	2.3	-0.5	3.56	1.44
3	14	85	75	1.6	-0.5	3.58	1.70
4	13	66	55	1.2	-0.5	3.60	1.99
5	13	52	42	0.9	-0.5	3.61	2.25

TABLE II: The total energies of the FM, C, G-type antiferromagnetism states, relative to that of the A-AFM, the exchange constant in the a-b plane (J_{ab}) and that along the c-axis (J_c); the magnetic moment of Cr ion, the occupation numbers of $d_{3z^2-r^2}$ (Occ-($_{3z^2-r^2}$)) and $d_{x^2-y^2}$ (Occ-($_{x^2-y^2}$)) and the band gap (in A-AFM state).

U_{eff}	FM(meV)	C(meV)	G(meV)	J_{ab}(meV)	J_c(meV)	Cr (μ_B)	Occ-($_{3z^2-r^2}$)	Occ-($_{x^2-y^2}$)	gap (eV)
0	-76	191	180	4.3	1.3	3.58	0.50	0.50	
1	-81	171	161	4.0	1.4	3.60	0.40	0.60	
2	-10	109	126	2.4	0.5	3.60	0.15	0.85	
3	14	85	70	1.4	-0.6	3.61	0.09	0.91	0.588
4	12	64	52	1.0	-0.5	3.62	0.00	1.00	0.888
5	11	55	43	0.8	-0.4	3.63	0.00	1.00	1.182